



HAL
open science

Estimating surface soil moisture over Sahel using ENVISAT radar altimetry

Christophe Fatras, Frédéric Frappart, Éric Mougin, Manuela Grippa, Pierre
Hiernaux

► **To cite this version:**

Christophe Fatras, Frédéric Frappart, Éric Mougin, Manuela Grippa, Pierre Hiernaux. Estimating surface soil moisture over Sahel using ENVISAT radar altimetry. *Remote Sensing of Environment*, 2012, 123 (8), pp.496-507. 10.1016/j.rse.2012.04.013 . hal-00743876

HAL Id: hal-00743876

<https://hal.science/hal-00743876>

Submitted on 21 Oct 2012

HAL is a multi-disciplinary open access archive for the deposit and dissemination of scientific research documents, whether they are published or not. The documents may come from teaching and research institutions in France or abroad, or from public or private research centers.

L'archive ouverte pluridisciplinaire **HAL**, est destinée au dépôt et à la diffusion de documents scientifiques de niveau recherche, publiés ou non, émanant des établissements d'enseignement et de recherche français ou étrangers, des laboratoires publics ou privés.

1
2
3
4
5
6
7
8
9
10
11
12
13
14

**Estimating surface soil moisture over Sahel
using ENVISAT radar altimetry**

C. Fatras, F. Frappart*, E. Mougin, M. Grippa, P. Hiernaux

**Université de Toulouse, OMP, GET (UMR 5563 CNRS-UPS-IRD)
14 avenue Edouard Belin 31400 Toulouse – France**

*Corresponding author: Géosciences Environnement Toulouse (GET)
Observatoire Midi-Pyrénées
14 avenue Edouard Belin 31400 Toulouse, France
E-mail address: christophe.fatras@get.obs-mip.fr (Christophe Fatras)

15
16
17

ABSTRACT

18 This paper analyses the potential of the radar altimeter onboard ENVISAT for
19 estimating surface soil moisture in the semi-arid Gourma region in Northern Mali. To this
20 end, the relationships between observed backscattering coefficients derived from 4 retracking
21 algorithms, namely Ocean, Ice-1, Ice-2 and Sea-Ice, and ground data, including soil type,
22 topography, vegetation and soil moisture are investigated. The considered period is 2002-
23 2010. Results show a strong linear relationship between the backscattering coefficients and
24 surface soil moisture measured at six different stations along the satellite track. The best
25 results are obtained with the Ice-1 and Ice-2 algorithms. In these cases, correlation
26 coefficients are higher than 0.8 with RMSE smaller than 2%. Vegetation effects are found to
27 be small due both to the nadir-looking configuration of the radar altimeter and to the low
28 vegetation cover. Finally, the relationship between soil moisture and normalized
29 backscattering coefficient is used to retrieve soil moisture from the altimeter data. These
30 estimates are then compared to soil moisture estimations obtained from the METeorological
31 Operational (METOP) Advanced SCATterometer (ASCAT). These results highlight the high
32 capabilities of Ku-band altimeters to provide an accurate estimation of surface soil moisture in
33 semiarid regions.

34
35

Keywords: surface soil moisture; radar altimetry; backscattering coefficient; Sahel

36 **1. Introduction**

37 In the Sahelian region of West-Africa, soil moisture drives many surface processes
38 including soil organic matter mineralization (e.g. [Zech et al., 1997](#)), vegetation productivity
39 (e.g. [Hiernaux et al., 2009](#)), land surface fluxes (e.g. [Brümmer et al., 2008](#)) and land surface-
40 atmosphere interactions (e.g. [Taylor et al., 2010](#)). Particularly, the Sahel is identified as one of
41 the regions of the world with the strongest feedbacks between soil moisture and precipitation
42 ([Koster et al., 2004](#)). Monitoring of the spatio-temporal variability of soil moisture is
43 therefore an important issue within the frame of the AMMA (*African Monsoon*
44 *Multidisciplinary Analysis*) project which aims at providing a better understanding of the
45 West African Monsoon and its physical, chemical and biological environments ([Redelsperger](#)
46 [et al., 2006](#)).

47 Active microwave remote sensing has demonstrated considerable capabilities in
48 estimating surface soil moisture (SSM), in semi-arid regions (e.g. [Wagner and Scipal, 2000](#);
49 [Mladenova et al., 2010](#)). The potential of radar sensors for detecting changes in SSM results
50 from their high sensitivity to the variation of surface dielectric properties that are mainly
51 linked to changes in SSM. Moreover, in semi-arid regions, observations made at low
52 incidence angles are found to be strongly correlated to SSM because vegetation effects are
53 minimized ([Tansey et al., 1999](#); [Moran et al., 2000](#); [Baup et al., 2007](#)).

54 Initially designed to make accurate measurements of the sea surface topography,
55 satellite radar altimetry (RA) has been successfully employed to derive valuable information
56 for land hydrology by providing an estimation of water level variations of lakes ([Birkett,](#)
57 [1995](#); [Cazenave et al., 1997](#); [Crétaux et al., 2009](#)), rivers ([Birkett, 1998](#); [Birkett et al., 2002,](#)
58 [Frappart et al., 2006a](#)) and floodplains ([Frappart et al., 2005](#); [2006b](#); [Santos da Silva et al.,](#)
59 [2010](#)). The magnitude of RA backscattering coefficients σ_0 provided by the
60 TOPEX/POSEIDON altimeter mission at Ku- and C- bands, and by the European

61 ENVIRONMENTAL SATellite (ENVISAT), at Ku and S bands, is related to the dynamics of
62 surface properties (e.g. [Papa et al., 2003](#); [Legrésy et al., 2005](#)). Particularly, spatial and
63 temporal variations of RA backscattering coefficients are found to be related to soil roughness
64 and surface soil moisture (SSM) changes in the Sahara and Australian deserts ([Cudlip et al.,
65 1994](#); [Ridley et al., 1996](#)). Moreover, a semi-empirical model was recently proposed to
66 estimate SSM using RA backscattering coefficients over semi-arid surfaces ([Bramer et al.,
67 2010](#)). Comparisons were made with soil moisture outputs from a hydrological model
68 showing a link between modeled and altimetry derived soil moisture. Radar altimeters are a
69 priori suitable to SSM retrieval since attenuation by the vegetation layer is minimized by their
70 nadir-looking configuration. This is particularly true in semi-arid regions where vegetation
71 cover is sparse. However, their potentials for SSM retrieval have not been demonstrated yet.

72 The objective of the present study is to investigate whether the backscattering coefficient
73 delivered by radar altimetry can be used to provide an accurate estimation of surface soil
74 moisture over semi-arid areas. To this end, the data acquired by the ENVISAT RA-2 over
75 Northern Sahel in Mali are analyzed over the 2002-2010 period and relationships are
76 investigated between observed backscattering coefficients and ground data including soil
77 type, topography, vegetation and soil moisture acquired at six different stations along the
78 satellite track. For the sandy soils sites, a linear relationship is derived between the altimetry
79 backscatter and the in situ SSM. Finally, this relationship is used to retrieve soil moisture
80 from the altimeter data and the resulting soil moisture estimate is compared to the estimate
81 obtained from the METeorological Operational (METOP) Advanced SCATterometer
82 (ASCAT).

83

84 **2. Study area and data**

85 *2.1. The study site*

86 The African Monsoon Multi-disciplinary Analysis – Couplage de l'Atmosphère
87 Tropicale et du Cycle Hydrologique (AMMA-CATCH) meso-scale site is located in the
88 Gourma region (1°W-2°W, 14.5°N-17.5°N) in Mali (Fig. 1), and stretches from the loop of
89 the Niger River southward down to the country border with Burkina-Faso (Mougin et al.,
90 2009). This site is entirely located within the Sahel bioclimatic zone and is bracketed by the
91 150 and 500 mm annual isohyets. The rain distribution is strictly mono-modal with rainfall
92 starting in June and ending in September with a maximum in August (Frappart et al., 2009).
93 During the wet season, rangeland vegetation is composed of a low herbaceous layer
94 dominated by annuals and a sparse woody plant population (canopy cover <5%). Annual
95 herbs germinate with the first significant rains, in June or July, and unless the plants wilt
96 before maturity owing to a lack of rainfall, the senescence coincides approximately with the
97 end of the rainy season. This short rainy season is followed by a long dry season during which
98 there is no green vegetation except for rare perennial herbaceous and the foliage of some of
99 scattered trees and shrubs.

100 The Gourma region is a vast peneplain at between 250 and 330 m altitude with highest
101 isolated sandstone buttes reaching 900-1100 m close to the town of Hombori. The eroded and
102 exposed rock-surfaces (23% of the whole area) are locally capped by iron pan but larger areas
103 of the region (58%) are covered by deep and fixed sand. At meso-scale, predominantly sandy
104 or shallow soils distribute in large alternant swaths of contrasted land cover (Fig. 1). Besides
105 these two major landforms, remnants of alluvial systems and lacustrine depressions form a
106 web of narrow valleys often slotted in between sandy and shallow soils.

107 The overall observation strategy of the AMMA-CATCH site is based on the
108 deployment of a variety of instrument networks, from local- to meso-scales, dedicated to the
109 monitoring and documentation of the major variables characterizing the climate and the
110 spatio-temporal variability of geophysical and land surface variables. Long term

111 measurements monitor meteorological variables, vegetation and surface hydrology including
112 soil moisture.

113

114 *2.2 Surface soil moisture measurements*

115

116 Six automatic soil moisture stations are located at the vicinity of the ENVISAT's path
117 #302 (Fig. 1). These stations are part of the soil moisture network set up from 2005 within the
118 frame of the AMMA project (de Rosnay et al., 2009). Characteristics (name, location, date of
119 installation, soil type, sensor depth) of the 6 soil moisture stations are given in Table 1. The
120 same installation protocol is used for all the soil moisture stations equipped by Time Domain
121 Reflectometry sensors (Campbell Scientific CS616) that provide measurements at 15 min
122 time step, except for the the Eguerit erosion surface site where delta-T sensors have been
123 installed. Sensors are calibrated by using in situ gravimetric measurements and estimation of
124 soil bulk density. Only surface measurements recorded at 5, 10, 30 and 40 cm depth are
125 considered here in agreement to the microwave soil penetration depth (Ulaby et al., 1981). In
126 the following, Surface Soil Moisture (SSM) data are expressed in volumetric water content
127 ($\text{m}^3 \text{m}^{-3}$). Local SSM data typically range between 0.05% (dry season) and 28% (wet season)
128 for the sandy soils.

129

130 *2.3 ENVISAT RA-2 backscattering coefficients*

131 In the framework of its Earth observation programme, the European Space Agency
132 (ESA) launched the ENVironmental SATellite (ENVISAT) satellite on February 2002.
133 ENVISAT carries 10 scientific instruments which provide atmosphere, ocean, land, and ice
134 measurements, including a nadir-pointing radar altimeter (RA-2 or Advanced Radar
135 Altimeter) (Wehr & Attema, 2001). ENVISAT flies in a sun-synchronous polar orbit at an

136 altitude of about 800 km, with a 35-day repeat cycle and an inclination of 98.6°, providing
137 observations of the Earth surface (ocean and land) from 81.5° latitude North to 81.5° latitude
138 South, with a ground-track spacing of around 80 km at the Equator. RA-2 is a nadir-looking
139 pulse-limited radar altimeter operating at two frequencies at Ku- (13.575 GHz / 2.3 cm of
140 wavelength) and S- (3.2 GHz / 9.3 cm) bands (Zelli, 1999). Its main characteristics are
141 summarized in Table 2. The diameter of the pulse-limited footprint are respectively 3.4km in
142 Ku and 4.8km in S bands (ESA, 2002). However, the surface footprint size is uncertain and its
143 nominal diameter varies approximately between 2km and 10km for Ku band (Chelton et al.,
144 2001; Peacock & Laxon, 2004). These variations are caused by the topography and the
145 inhomogeneities of the surface. Over flat surfaces, an approximate radius of 2 km is generally
146 considered as a good approximation for Ku band (Chelton et al., 2001). Over land, the
147 presence of open water in the footprint produces strong specular reflections that can be off-
148 nadir. The returned signal can be dominated by these off-nadir reflections causing tracking
149 errors (altimeter mispointing) even if they are off-nadir by several (1-10) km for Ku band, and
150 beyond for S band due to a larger beam width. Processing of radar echoes or altimeter
151 waveforms is performed on the ground to obtain range values, *i.e.* the distance between the
152 satellite and the surface estimated from the round-trip time of the electromagnetic pulse, and
153 backscattering coefficients σ_0 derived from the power of the altimeter return pulse. The
154 Geophysical Data Records (GDRs) distributed by ESA (ESA, 2002) include accurate satellite
155 positions (longitude, latitude and altitude of the satellite on its orbit) and timing, altimeter
156 ranges, instrumental, propagation and geophysical corrections applied to the range, and
157 several other parameters such as the backscattering coefficients. For the ENVISAT mission,
158 four different retracking algorithms are operationally applied to RA-2 raw-data to provide
159 range estimates and backscattering coefficients. Each retracking algorithm namely Ocean
160 (Brown, 1977; Hayne, 1980), Ice-1 (Wingham et al., 1986; Bamber, 1994), Ice-2 (Legrésy,

161 1995; Legrésy and Rémy, 1997) and Sea-Ice (Laxon, 1994) has been developed for a specific
162 type of surface but none of them has been specifically designed for processing altimeter
163 echoes over land. The backscattering coefficient is directly related to the integral against time
164 of the radar echo or waveform. Ocean and Ice-2 algorithms are based on the fit of a
165 theoretical waveform shape corresponding to sea and ice cap surfaces to estimate precisely the
166 position of the leading front of the waveform. The value of the backscattering coefficient is
167 determined by integration of the theoretical waveform. For Ice-1 and Sea Ice these parameters
168 are estimated empirically using thresholds on the amplitude of the waveform. The errors on
169 the estimated σ_0 (instrument noise, orbit variations, atmosphere interferences) are expected to
170 be lower than 0.29 dB in Ku band and 0.37 dB in S band (Pierdicca et al., 2006).

171 The variables used in this study, include the satellite positions, times of acquisition,
172 the 1 Hz Ocean-retracked (Ku and S bands), the 18 Hz Ice-1, Ice-2 (Ku and S bands), and the
173 18 Hz Sea Ice (Ku band) backscattering coefficients measured at 23.8 and 36.5 GHz
174 contained in the ENVISAT RA-2 GDRs made available by the Centre de Topographie des
175 Océans et de l'Hydrosphère (CTOH - <http://ctoh.legos.obs-mip.fr/>) for the ground track #302
176 over the AMMA mesoscale site in Gourma (see Fig.1). The considered period is September
177 2002 – October 2010 (8 years). However, S-band data are only available until January 2008
178 (5.4 years).

179

180 2.4 ASCAT SSM products

181 The METeorological Operational (METOP) Advanced SCATterometer (ASCAT) is
182 the enhanced successor of the scatterometers flown on the European Remote Sensing (ERS-1
183 and ERS-2) satellites. ASCAT operates at C-band (5.255 GHz) with VV polarization. Two
184 triplets of spatially averaged backscattering coefficient values at a spatial resolution of around
185 30 and 50 km for each location along the swath are derived from continuous observations

186 performed by three radar antenna beams at three different azimuth angles (45°, 90°, and 135°
187 sideward from the direction of the satellite motion) on both side of the METOP satellite
188 (Naeimi et al., 2009). Technical information concerning ASCAT measurements are presented
189 in Table 3. SSM products based on these observations are then generated using the SSM
190 retrieving algorithm developed by Wagner (1998) from ERS data. The backscattering
191 coefficients are first normalized to a standard incidence of 40°, and then inverted into SSM
192 assuming a linear relationship between these two quantities. In this study, we use the
193 interpolated SSM products given at a resolution of 30 km following a nodal grid of 12.5 km,
194 which correspond to the closest time to the altimetry measurements (with a variation from a
195 few minutes to 18h), for the period June 2007 - October 2010.

196

197 *3. Spatio-temporal variations of RA-2 backscattering coefficients*

198 Along-track profiles (Fig. 2) of σ_0 in Ku- and S- bands are averaged at each satellite
199 pass at a spatial resolution of 0.008° (~1km) for the rainy (JJAS) and the core of the dry
200 (JFMA) seasons for Ocean, Ice-1, Ice-2, and Sea Ice retracking algorithms over the
201 ENVISAT RA-2 groundtrack #302 between latitudes 14.5° and 16.25°. This spatial resolution
202 is chosen as it captures the spatial heterogeneity of the surface (Mougin et al., 2009) and of
203 the local soil moisture condition (Baup et al., 2007; de Rosnay et al., 2009). It corresponds to
204 three different 18 Hz measurements which footprint centers are separated by 370 m for Ice-1,
205 Ice-2, and Sea Ice σ_0 , and one 1 Hz measurements (corresponding to a distance of 7.5 km) for
206 Ocean σ_0 .

207 In the followings, only the results obtained with the Ice-1 retracking algorithm are
208 displayed. Results using the three other retracking algorithms are cited and discussed in the
209 text.

210

211 *3.1 Backscattering coefficient seasonal variations along the latitudinal transect*

212 The extrema values reached per grid cell over the whole observation periods by σ_0 for
213 Ku-band (8years) and S-band (5.4years) are identified for the Ice-1 processing during the wet
214 seasons (June to September) and the core of the dry season (January to April). Similar profiles
215 are obtained for Ku and S bands with a lower dynamics for the S band in general, especially
216 over sandy areas. The spatial σ_0 dynamics during the dry season is slightly larger for S-band
217 than for Ku-band. On the contrary, the spatial dynamics during the wet season is lower for S-
218 band than for Ku-band. This can be due both to the larger footprint of S band that
219 encompasses surfaces of different types (i.e., mix between rocky, sandy and clay soils, or
220 presence of permanent ponds far from nadir that have a signature in S but not in Ku bands)
221 and to a lower sensitivity of the S band (wavelength of 9 cm) to changes in surface roughness.
222 Lower values of backscattering coefficients are generally observed over sandy surfaces (fixed
223 dunes) whereas higher values are found over rocky surfaces (erosion surfaces) and surfaces
224 containing temporary open water (ponds and wadi). The higher surface roughness of the
225 sandy surfaces could account for a smaller backscattering response in the nadir direction. The
226 yearly amplitude of the backscattered signal exhibits large variations along the latitudinal
227 transect, from 10 to 30 dB for Ku-band and from 10 to 20dB for S-band over sandy surfaces,
228 from 15 to 30 dB for Ku-band and from 15 to 20dB for S-band over erosion rocky surfaces,
229 and reaches 45 dB over water bodies for both bands, as illustrated by the response of the Ekia
230 wadi (16.05° N).

231 Similar along-track profiles are obtained with the other retracking algorithms.
232 However the profiles established with Ocean are smoother as only 1 Hz data are available
233 with this processing.

234

235 *3.2 Spatio-temporal variations along the latitudinal transect*

236 The latitudinal variations of the backscattering coefficient from the track #302 are
237 plotted as a function of time over the 2002-2010 period for Ku-band (Fig. 3a) and over the
238 2002-2007 period for S-band (Fig. 3b). They both exhibit a well-marked seasonality with
239 higher values of σ_0 during the rainy season, particularly at latitudes above 15.4°N where
240 rocky soil types and ponds are more important. However, for the same type of surface, the
241 values are generally higher in the South than in the North in agreement with the rainfall
242 gradient (Frappart et al., 2009). During the wet season, three zones in the North (around
243 15.75°, 16.1° and 16.2° of latitude) present very strong backscattering coefficients at both
244 frequencies. They correspond to the temporarily open waters of Quart Fotou valley, Ekia wadi
245 and Karouassa valley. High σ_0 values are observed over wide portions of the latitudinal
246 transect for several annual cycles. They can be related to rainfall events affecting the whole or
247 large parts of the Gourma region as for example the strong rainfalls that occurred on August
248 11th, 2006 simultaneously with ENVISAT cycle 50 and the rainfall on June 26th, 2009 a few
249 hours before ENVISAT cycle 80.

250

Figure 3

251 Besides, locally harsh topography affects data availability. The retracking algorithms based on
252 modeling of the surface response (Ice-2 and Ocean) are unable to provide valid data over the
253 erosion surface at 15.15° of latitude, and at the vicinity of the Hombori mounts (15.3° of
254 latitude). This is likely due to the inability to fit the parameters of theoretical waveforms on
255 the observed ones whereas the empirical retracking processes (centre of gravity for Ice-1 and
256 maximum for Sea Ice of the waveform) are more robust.

257

258 **4. Surface soil moisture estimation**

259 *4.1 Relationship between backscattering coefficient and SSM*

260 In this section, the time variation of RA backscattering coefficients at the vicinity of
261 the 6 *in situ* soil moisture stations (Ekiá, Eguerit, Bangui Mallam, Agoufou, Kyrnia and
262 Kobou) are analyzed and compared to the temporal variation of SSM measured *in situ*.

263 Two methods are used to build time series of backscattering coefficients at the vicinity
264 of a ground soil moisture station. The first approach is based on the definition of a rectangular
265 window of a few kilometers width around the nominal altimeter track corresponding to an
266 area homogeneous in soil texture and topography. To obtain the backscattering coefficients
267 time series, all the measurements that fall within this window are averaged for each cycle.
268 This method is similar to the one used to derive water levels of rivers and lakes from radar
269 altimetry data (e.g. Frappart et al., 2006a). The second approach consists in selecting the
270 backscattering coefficient data the closest from the soil moisture site. However, at Ekiá site
271 (see Fig.1 and Table 1), the selected data are the closest from a location 7 km to the South-
272 west of the site instead, in order to minimize the effect of the presence of a temporary pond
273 northward of the soil moisture site. The results presented below are obtained using the second
274 approach that provides better results (*i.e.* higher correlation and lower RMSE).

275 The backscattering coefficients for Ku- and S- bands display a strong seasonality.
276 Maxima of σ_0 are observed during the peak of the rainy season in close relation with SSM
277 content measured at 5 and 10 cm depths, as illustrated for the Agoufou site for the Ice-1
278 algorithm (Fig. 4).

279

Figure 4

305 are located in large fixed sandy dunes with low and gentle elevation changes (a few meters).
306 The closer to the ENVISAT track the measurements site, the better the correlation is.
307 Correlation coefficients of 0.95 and 0.86 and RMSE of 1.98% and 1.74% are obtained
308 between 5cm depth SSM and Ice-1 estimated σ_0 for short distances of 2 – 3 km (Eguerit and
309 Agoufou) whereas correlation coefficients (RMSE) range from 0.7 to 0.52 (3.61% to 5.84%)
310 for distances larger than 5.5 km (Bangui Mallam, Ekia and Kobou). The poor results obtained
311 at the Kyrnia site located at only 3 km from the altimeter swath are likely due to the presence
312 of a temporary pond close to the site. Overall, the results are quite similar for SSM measured
313 at 5 and 10 cm depth, as a mark of the soil moisture homogeneity close to soil surface. Similar
314 results are found with Ice-2 and Sea Ice based σ_0 . Overall, lower performances are obtained
315 for Ocean processed data as no high frequency data (18 Hz) are available.

316 **Figure 6**

317 Scatterplots of backscattering coefficients as a function of measured SSM (**Fig. 6**)
318 sometime display very high values of σ_0 (> 30 dB) that do not correspond to high SSM
319 measured in situ (see for example **Figs 6e-6f**). These off layers can be related to strong rainfall
320 events that took place a couple of hours before the altimeter overpass (e.g. on June 26th, 2009)
321 generating temporary puddles that enhanced the radar signal. In the case of Bangui Mallam, *in*
322 *situ* soil moisture measurements are not available after mid-July 2008 at 5cm depth.

323

324 *4.2 Effect of seasonal dynamics of vegetation on SSM estimation*

325 To determine whether the presence of vegetation affects the SSM – σ_0 relationships the
326 variation of Ice-1 estimated σ_0 is plotted against the measured Leaf Area Index (LAI) during
327 the 2005 - 2010 growing seasons for the Agoufou site. Methodology of LAI in situ
328 measurements are detailed in [Mougin et al. \(2012\)](#). The maximum corresponding herbaceous
329 vegetation cover at the Agoufou site is about 50%.

Figure 7

330
331 For LAI>0.2, the backscattering coefficient decreases (< 2 dB) as the LAI increases with a
332 correlation coefficient of -0.6 suggesting a weak attenuation of the radar wave by the
333 vegetation layer. The impact of vegetation remains anyway small because (i) the radar
334 altimeter is a nadir-looking instrument which means that the electromagnetic field crosses less
335 vegetation (smaller canopy optical thickness) than side-looking radars (SAR or scatterometer)
336 that observe the surface at angles greater than 10°, (ii) the Sahelian vegetation cover remains
337 low even at the peak of the wet season (except in seasonally flooded forests that are not
338 considered here).

339 For low LAI (LAI< 0.2) the observed increase of the backscattering coefficient with LAI
340 could be attributed to an enhancement of the scattering by the vegetation layer as already
341 observed on crops by [Ulaby et al. \(1984\)](#).

342

343 *4.3 Linear regression and SSM estimation*

344 Based on the experimental relationships displayed in [Fig. 6](#), a general linear regression
345 is established between normalized σ_0 and SSM for the sandy soils dominant across the
346 Gourma mesoscale window (58 % of the whole surface). Coefficients of the linear regression
347 between normalized backscattering coefficients and *in situ* SSM measurements for the three
348 sandy sites (Agoufou, Bangui Mallam and Ekia,) are determined and averaged ([Fig. 8](#)).
349 Following the methodology proposed by [Wagner and Scipal \(2000\)](#) and [Zribi et al. \(2007\)](#),
350 the normalized backscattering coefficients is calculated as the difference between the actual
351 backscattering value and the mean backscattering value estimated over the core of the dry
352 season (January to April) for each site. Indeed, the normalized backscattering coefficients
353 reflect the radar dynamics of the different surface types.

354 Finally, altimeter-derived SSM time series are estimated by inverting the general
355 linear relationship between backscattered and SSM established on sandy soils, for both 5cm
356 and 10cm depths.

357 **Figure 8**

358 Comparisons between *in situ* and altimetry-derived SSM are analyzed for the sandy sites
359 using the four retracking algorithms. Results of these comparisons (RMSE and correlation
360 coefficients) are summarized in **Table 6** and an example of time series of altimetry-derived
361 SSM is given for the Agoufou site (**Fig. 9**). The error introduced by the inverse function in the
362 SSM derived from σ_0 is 0.4% SSM obtained as the ratio between the error on σ_0 (maximum
363 value of 0.3 dB according to [Pierdicca et al., 2006](#)) and the slope of the mean linear
364 regression.

365 **Figure 9**

366 *4.4 Comparisons with ASCAT-derived SSM estimates*

367 To compare the ASCAT derived SSM products at a resolution of 35 km to the
368 ENVISAT RA-2 derived estimates, correlation coefficients have been calculated. For each
369 product, the reference point is the location of the in-situ measurement site. Hence the
370 ASCAT-derived SSM chosen for each study site is the one of the pixel containing the
371 reference point. Outliers in the ASCAT-derived SSM are filtered out using a threshold of 30%
372 of SSM. All the values of ENVISAT RA-2 derived SSM that fall within the ASCAT pixel
373 corresponding to the site (see 4.1) are averaged. Consequently, at a given time, between 80
374 and 100 backscattering coefficients are taken into account. The acceptable time offset
375 between ASCAT measurements and ENVISAT RA-2 data has been limited to 18hours.

376 Comparisons between altimetry derived SSM (for both 5cm and 10cm inverse
377 functions) and ASCAT SSM products are performed for the measurements sites of Agoufou,

378 Bangui Mallam, and Ekia. For the Agoufou site the time series are established from May 2007
379 to October 2010 (Fig.10), the common period of availability of the ASCAT and ENVISAT
380 data. The altimetry-derived SSM averaged over the ASCAT pixel exhibit similar temporal
381 variations in phase with ASCAT-based SSM but with large difference of amplitudes reaching
382 up to 12% m^3m^{-3} of SSM. The correlation coefficients and RMSE calculated between the four
383 different altimetry-based and ASCAT-derived SSM for the three selected sites (Table 7)
384 exhibit large variations from one region to another with correlations around 0.5 for Agoufou,
385 0.4-0.5 for Ekia and only 0.3-0.4 for Bangui Mallam, and RMSE lower than 5% except at
386 Ekia. These discrepancies can be accounted for the widely different scales observed by each
387 sensor. ASCAT-based estimates are representative of larger areas ($\sim 1,200\text{km}^2$) than
388 ENVISAT-derived SSM ($\sim 250\text{km}^2$) using the ENVISAT integration over the ASCAT pixel.

389 **Figure 10**

390

391 **5. Conclusion**

392 This study has shown that backscattering coefficients at Ku- obtained from ENVISAT
393 RA-2 data can be related to the temporal variation of moisture content in the upper soil
394 profile. In situ SSM measurements and backscattering coefficients have been found generally
395 well correlated, even if the quality of the relationships highly depends on i) the distance
396 between the measurement site and the altimeter track, ii) the presence of open water in the
397 altimeter footprint, iii) the topography of the site and the retracking algorithm. The best
398 results are obtained for backscattering coefficients processed with Ice-1, Ice-2, and Sea-Ice
399 algorithms compared to the Ocean retracking algorithm as no 20 Hz measurements are
400 available with the latter one. A linear relationship between radar altimetry backscattering
401 coefficients and SSM is established for the dominant sandy sites, similar to the ones

402 previously found using ENVISAT-ASAR data over the same study area (see Baup et al.,
403 2007; 2011). Only a small attenuation by the vegetation cover is found allowing SSM to be
404 accurately estimated from radar altimetry data without any correction. To our knowledge, this
405 is the first demonstration of the potentialities of radar altimetry to derive surface soil moisture
406 in a semi-arid environment.

407 Comparisons of altimetry derived SSM with low spatial resolution SSM products
408 obtained from ASCAT scatterometer data show reasonable correlation between the two
409 satellite-derived estimates. Radar altimetry-based SSM products offer new and
410 complementary information to relate the local (*in situ*) to the regional (~25 km) scales, and
411 demonstrate a strong potential to evaluate low resolution satellite SSM products to be used in
412 a down-scaling approach.

413 Improvements of altimetry derived SSM are expected from the use of higher spatial
414 resolution altimetry data such as those that will be provided by the French-Indian AltiKa radar
415 altimetry mission to be launched in August 2012.

416

417

418 **Acknowledgements**

419 This work was performed within the framework of the AMMA project. Based on a French
420 initiative, AMMA has been constructed by an international group and is currently funded by
421 large number of agencies, especially from France, the UK, the US and Africa. It has been the
422 beneficiary of a major financial contribution from the European Community's Sixth
423 Framework Research Programme. Detailed information on the scientific coordination and
424 funding is available on the AMMA international web site (<https://www.amma-eu.org/>). This
425 work was funded by the Programme National en Télédétection Spatiale (PNTS) in the

426 framework of the project “Potentialités des altimètres radars spatiaux pour l’hydrologie en
427 zone sahélienne. Perspectives pour la mission SWOT”.

428 The authors thank the Centre de Topographie des Océans et de l’Hydrosphère (CTOH) at
429 Laboratoire d’Etudes en Géophysique et Océanographie Spatiales (LEGOS), Observatoire
430 Midi-Pyrénées (OMP), Toulouse, France for providing the ENVISAT RA-2 GDR dataset
431 used in the present study.

432

433

434 **References**

- 435 Bamber, J. L. (1994). Ice sheet altimeter processing scheme. *International Journal of Remote*
436 *Sensing*, 15(4), 925–938.
- 437 Baup F., Mougin E., de Rosnay P., Timouk F., Chênerie I. (2007). Surface soil moisture
438 estimation over the AMMA Sahelian site in Mali using ENVISAT/ASAR data.
439 *Remote Sensing of Environment*, 109(4), 473–481.
- 440 Baup F., Mougin E., de Rosnay P., Hiernaux P., Frappart F., Frison P.L., Zribi M., Viarre J.
441 (2011). Mapping surface soil moisture over the Gourma mesoscale site (Mali) by
442 using ENVISAT-ASAR data. *Hydrology and Earth System Sciences*, 15, 603-616.
- 443 Birkett, C. M. (1995). The contribution of TOPEX/POSEIDON to the global monitoring of
444 climatically sensitive lakes. *Journal of Geophysical Research*, 100(C12), 25,179–
445 25,204.
- 446 Birkett, C. M. (1998). Contribution of the TOPEX NASA radar altimeter to the global
447 monitoring of large rivers and wetlands. *Water Resources Research*, 34(5), 1223–
448 1239.
- 449 Birkett, C. M., Mertes, L. A. K., Dunne, T., Costa, M. H., & Jasinski, M. J. (2002). Surface
450 water dynamics in the Amazon basin: Application of satellite radar altimetry. *Journal*
451 *of Geophysical Research*, 107(D20), 8059–8080.
- 452 Bramer, S.M.S., Berry, P.A.M., & Carter, J. (2010). The use of radar altimetry in soil
453 moisture monitoring in support of the SMOS mission. *Proceedings of Earth*
454 *Observation and Water Cycle Science, Frascati, Italy, 18–20 November 2009 (ESA*
455 *SP-674, January 2010)*.
- 456 Brown, G. S. (1977). The average impulse response of a rough surface and its applications.
457 *IEEE Transactions on Antennas and Propagation*, 25(1), 67–74.

458 Brümmer, C., Falk U., Papen H., Szarzynski J., Wassmann R., Brüggemann N. (2008).
459 Diurnal, seasonal, and interannual variation in carbon dioxide and energy exchange in
460 shrub savanna in Burkina Faso (West Africa). *Journal of Geophysical Research*, 113,
461 G02030, 11p., doi:10.1029/2007JG000583.

462 Cazenave, A., Bonnefond, P., & Do Minh, K. (1997). Caspian sea level from Topex/Poseidon
463 altimetry: Level now falling, *Geophysical Research Letters*, 25 (2), 155-158.

464 Chelton, B. C., Ries, J. C., Haines, B. J., Fu, L., & Callahan, P. S. (2001). Satellite altimetry.
465 In L. Fu & A. Cazenave (Eds.), *Satellite Altimetry and Earth Sciences: An Handbook*
466 *of Techniques and Applications* (pp. 1-131): Academic Press.

467 Crétaux, J.F., Calmant, S., Romanovski, V., Shibuyin, A., Lyard, F., Berge-Nguyen, M.,
468 Cazenave, A., Hernandez, F., & Perosanz, F. (2009). An absolute calibration site for
469 radar altimeters in the continental domain: lake Issykkul in Central Asia. *Journal of*
470 *Geodesy*, 83(8), 723-735.

471 Cudlip, W., Ridley, J.K., Strawbridge, F., Harris, A. and Rapley, C.G. (1994): Detecting
472 surface roughness and moisture variations in deserts. *Proceedings of the 2nd ERS-1*
473 *Symposium, Hamburg 1993, ESA SP-361*, 849-853.

474 de Rosnay P., Gruhier C., Timouk F., Baup F., Mougine E., Hiernaux P., Kergoat L., LeDantec
475 V. (2009). Multi-scale soil moisture measurements over the Gourma meso-scale site in
476 Mali. *Journal of Hydrology, AMMA CATCH special issue*, 375(1-2), 241–252.

477 ESA (2002). ENVISAT RA2/MWR Product handbook, *RA2/MWR products user guide*.

478 Frappart, F., Seyler, F., Martinez, J. -M., Leon, J. -G., & Cazenave, A. (2005). Floodplain
479 water storage in the Negro River basin estimated from microwave remote sensing of
480 inundation area and water levels. *Remote Sensing of Environment*, 99(4), 387–399.

481 Frappart, F., Calmant, S., Cauhopé, M., Seyler, F., & Cazenave, A. (2006a). Preliminary
482 results of ENVISAT RA-2-derived water levels validation over the Amazon basin.
483 *Remote Sensing of Environment*, 100(2), 252–264, doi:10.1016/j.rse.2005.10.027

484 Frappart, F., Do Minh, K., L'Hermitte, J., Cazenave, A., Ramillien, G., Le Toan, T., &
485 Mognard-Campbell N. (2006b). Water volume change in the lower Mekong from
486 satellite altimetry and imagery data. *Geophysical Journal International*, 167(2),
487 570–584, doi:10.1111/j.1365246X.2006.03184.x.

488 Frappart F., Hiernaux P., Guichard F., Mougin E., Kergoat L., Arjounin M., Lavenu F., Koité
489 M., Paturel J.E., Lebel T., 2009, Rainfall regime over the Sahelian climate gradient in
490 the Gourma, Mali. *Journal of Hydrology, AMMA CATCH special issue*, 375(1-2), 128-
491 142.

492 Hayne, G. S. (1980). Radar altimeter mean return waveforms from near normal-incidence
493 ocean surface scattering. *IEEE Transactions on Antennas and Propagation*, 28(5),
494 687–692.

495 Hiernaux, P., Mougin, E., Diarra, L., Soumaguel, N., Lavenu, F., Tracol, Y., Diawara, M.,
496 Jarlan, L. (2009). Rangeland response to rainfall and grazing pressure over two
497 decades: herbaceous growth pattern, production and species composition in the
498 Gourma, Mali. *Journal of Hydrology*, 375, 114-127.

499 Koster, R.D., Dirmeyer, P., Guo, Z., Bonan, G., Cox, P., Gordon, C., Kanae, S., Kowalczyk,
500 E., Lawrence, D., Liu, P., Lu, C., Malyshev, S., McAvaney, B., Mitchell, K., Mocko,
501 D., Oki, T., Oleson, K., Pitman, A., Sud, Y., Taylor, C., Verseghy, D., Vasic, R., Xue,
502 Y., Yamada, T. (2004). Regions of strong coupling between soil moisture and
503 precipitation. *Sciences*, 305, 1038–1040.

504 Laxon, S. (1994). Sea ice altimeter processing scheme at the EODC. *International Journal of*
505 *Remote Sensing*, 15(4), 915–924.

506 Legrésy B. (1995). Etude du retracking des surfaces des formes d'onde altimétriques au-
507 dessus des calottes, *rapport CNES, CT/ED/TU/UD96.188, contrat n°*
508 *856/2/95/CNES/006*, 81 pp.

509 Legrésy, B., & Rémy, F. (1997). Surface characteristics of the Antarctic ice sheet and
510 altimetric observations. *Journal of Glaciology*, *43(144)*, 197–206.

511 Legrésy, B., Papa, F., Rémy, F., Vinay, G., van den Bosch, M., & Zanife, O.Z. (2005).
512 ENVISAT radar altimeter measurements over continental surfaces and ice caps using
513 the ICE-2 retracking algorithm. *Remote Sensing of Environment*, *95*, 150-163,
514 doi:10.1016/j.rse.2004.11.018.

515 Mladenova, I., Lakshmi, V., Walker, J.P., Panciera, R., Wagner, W., Doubkova, M. (2010):
516 Validation of the ASAR Global Monitoring Mode Soil Moisture Product Using the
517 NAFE'O5 Data Set. *IEEE Transaction on Geoscience and Remote Sensing*, *48*, 2498-
518 2508.

519 Moran, M. S., Hymer, D. C., Qi, J., Sano, E. E. (2000). Soil moisture evaluation using-
520 temporal synthetic aperture radar (SAR) in semiarid rangeland. *Agricultural and Forest*
521 *Meteorology* *105*, 69–80.

522 Mougin E., Lopes A., Frison P.L., Proisy C., 1995, Preliminary analysis of the ERS-1 wind-
523 scatterometer data over land surfaces. *Int. J. Remote Sensing*, *16(2)*, 391-398.

524 Mougin, E., Hiernaux, P., Kergoat, L., de Rosnay, P., Grippa, M., Timouk, F., Arjounin, M.,
525 Le Dantec, V., Demarez, V., Ceschia, E., Mougenot, B., Baup, F., Frappart, F., Frison,
526 P-L., Gardelle, J., Gruhier, C., Jarlan, L., Mangiarotti, S., Sanou, B., Tracol, Y.,
527 Guichard, F., Trichon, V., Diarra, L., Soumaré, A., Koité, M., Dembélé, F., Lloyd, C.,
528 Hanan, N.P., Damesin, C., Delon, C., Serça, D., Galy-Lacaux, C., Seghiéri, J.,
529 Becerra, S., Dia, H., Gangneron, F., Mazzega, P. (2009). The AMMA-CATCH
530 Gourma observatory site in Mali: Relating climate variations to changes in vegetation,

531 surface hydrology, fluxes and natural resources, *Journal of Hydrology*, 375(1-2), 14-
532 33, doi:10.1016/j.hydrol.2009.06.0045

533 Mougin, E., Demarez, V., Hiernaux, P., Diawara, M., Berg, A. (2012) Estimation of LAI,
534 fCover and fAPAR of a Sahelian grassland (Gourma, Mali). Submitted to *Agricultural*
535 *and Forest Meteorology*.

536 Naeimi, V., Scipal, K., Bartalis, Z., Hasenauer, S., & Wagner, W. (2009). An improved soil
537 moisture retrieval algorithm for ERS and METOP scatterometer observations. *IEEE*
538 *Transactions on Geoscience and Remote Sensing*, 47(7), 1999–2013,
539 doi:10.1109/TGRS.20082011617.

540 Papa, F., Legrésy, B., & Rémy, F. (2003). Use of the Topex-Poseidon dual-frequency radar
541 altimeter over land surfaces. *Remote Sensing of Environment*, 87, 136-147,
542 doi:10.1016/S0034-4257(03)00136-6.

543 Peacock, N. R., & Laxon, S. W. (2004). Sea surface height determination in the Arctic Ocean
544 from ERS altimetry. *Journal of Geophysical Research-Oceans*, 109, C07001.

545 Pierdicca, N., Greco, B., Bignami, C., Ferrazzoli, P., Mattioli, V. & Pulvirenti, L. (2006). The
546 calibration of the Envisat radar altimeter by a passive technique, *IEEE Transactions*
547 *on Geoscience and Remote Sensing*, 44(11), 3297–3307.

548 Redelsperger, J.-L., Thorncroft, C., Diedhiou, A., Lebel, T., Parker, D., Polcher, J.(2006)
549 African monsoon, multidisciplinary analysis (AMMA): an international research
550 project and field campaign. *Bulletin of the American Meteorological Society* 87(12),
551 1739–1746.

552 Ridley, J., Strawbridge, F., Card, R., & Phillips, H. (1996). Radar Backscatter Characteristics
553 of a Desert Surface, *Remote Sensing of Environment*, 57(2), 63-78.

554 Santos da Silva, J., Calmant, S., Seyler, F., Rottuno Filho, O.C., Cochonneau, G., &
555 Mansur, W.J.(2010). Water levels in the Amazon basin derived from the ERS 2 and

556 ENVISAT radar altimetry missions. *Remote Sensing of Environment*, 114(10), 2160-
557 2181, doi:10.1016/j.rse.2010.04.020.

558 Tansey, K. J., Millington, A. C., Battikhi, A. M., White, K. H. (1999). Monitoring soil
559 moisture dynamics using satellite imaging radar in northeastern Jordan. *Applied*
560 *Geography*, 19, 325-344.

561 Taylor, C.T., Harris, P. P., Parker, D. J. (2010). Impact of soil moisture on the development of
562 a Sahelian mesoscale convective system: a case-study from the AMMA Special
563 Observing Period. *Q. J. R. Meteorol. Soc.*, 136, 456-470.

564 Ulaby, F. T., Fung, A. K., Moore, R. K. (1981). Microwave and remote sensing active and
565 passive. *Norwood, MA: Artech House*.

566 Ulaby, F.T., Allen, C.T., Eger, G., and Kanemasu, E. (1984). Relating the microwave
567 backscattering coefficient to Leaf Area Index. *Remote Sensing of Environment*, 14,
568 113-133.

569 Wagner, W. (1998). Soil moisture retrieval from ERS scatterometer data. PhD dissertation,
570 Institute for Photogrammetry and Remote Sensing, Vienna, University of Technologu,
571 111p.

572 Wagner, W., and Scipal, K. (2000): Large-scale Soil moisture mapping in western Africa
573 using the ERS Scatterometer. *IEEE Transaction on Geosciences and Remote Sensing*
574 38, 1777-1782.

575 Wehr, T., & Attema, E. (2001). Geophysical validation of ENVISAT data products. *Advances*
576 *in Space Research*, 28(1), 83–91.

577 Wingham, D. J., Rapley, C. G., & Griffiths, H. (1986). New techniques in satellite altimeter
578 tracking systems. *Proceedings of IGARSS'86 Symposium, Zürich, 8–11 Sept. 1986*,
579 *Ref. ESA SP-254* (pp. 1339–1344).

580 Zech W., Senesi N., Guggenberger G., Kaiser K., Lehmann J., Miano T.M., Miltner A.,
581 Schroth G. (1997). Factors controlling humification and mineralization of soil organic
582 matter in the tropics. *Geoderma*, 79 (1-4), 117-161.

583 Zelli, C. (1999). ENVISAT RA-2 advanced radar altimeter: Instrument design and pre-launch
584 performance assessment review. *Acta Astronautica*, 44, 323–333.

585 Zribi, M., Andre, C., Saux-Picard, S., Descroix, L., Otle, C., Kallel, A. (2007). Soil moisture
586 mapping based on ASAR/ENVISAT radar data over a Sahelian region. *International*
587 *Journal of Remote Sensing*, 29, 3547-3565.

588

589 **Table captions**

590 Table 1 - Description of study sites and surface soil moisture (SSM) and precipitation data

591 Table 2 - ENVISAT RA-2 technical specifications

592 Table 3 - ASCAT technical specifications.

593 Table 4 – Correlation coefficient (r) and Root Mean Square Error (RMSE) between in-situ
594 measurement of surface soil moisture and S-band backscattering coefficients for the study
595 sites.

596

597 Table 5 - Correlation coefficient (r) and Root Mean Square Error (RMSE) between in-situ
598 measurement of surface soil moisture and Ku-band backscattering coefficients for the study
599 sites.

600

601 Table 6 - Correlation coefficient (r) and Root Mean Square Error (RMSE) between in-situ
602 measurement of surface soil moisture and Ku-band altimetry-derived surface soil moisture
603 estimation for the 3 sandy sites of Agoufou, Bangui Mallam and Ekia.

604

605 Table 7 - Correlation coefficients, bias and RMSE between ASCAT SSM products and RA-2
606 Ku-band derived SSM for 3 study sites (Agoufou, Bangui-Mallam and Ekia).

607

608

609
610
611
612
613
614

Table 1:

Description of study sites and surface soil moisture (SSM) and precipitation data

Site name	Agoufou	Bangui Mallam	Eguerit	Ekia	Kobou	Kyrnia	
Latitude	15.3453°	15.3978°	15.5026°	15.9651°	14.7284°	15.051°	
Longitude	-1.47913°	-1.34556°	-1.391°	-1.2534°	-1.502°	-1.546°	
Soil type	sand	sand, clay	rock	sand	sand, rock	sand, clay	
SSM	Period	2005 -2010	2005 -2010	2008 -2009	2005 -2010	2008 -2010	2007 -2010
	Depth (cm)	5, 10, 40	5*, 10, 30	5	5, 10, 30	5, 10, 30	5, 10, 30
	Resolution (min)	15	15	15	15	15	15
Rain gauge	Period	2005 -2010	2005 -2010	2008 -2009	2005 -2010	2005 -2010	2005 -2009
	Resolution (min)	5	5	5	5	5	5

615 *Measurements at 5cm are only available during the 2005-2008 period

616
617

618

Table 2:

619

ENVISAT RA-2 technical specifications

620

621

Repeat cycle	35 days
Altitude	782.4 - 799.8 km
Emitted frequencies (GHz)	(Ku) 13.575 - (S) 3.2
Antenna beam width (°)	(Ku) 1.29 - (S) 5.5
Backscatter maximum error (dB)	(Ku) 0.29 - (S) 0.37
Pulse-limited footprint diameter (km)	(Ku) 3.4 - (S) 4.8
Swath dispersion (km)	2

622

623

624

625
626
627
628
629

Table 3

ASCAT technical specifications

Altitude	~822km
Emitted frequencies (GHz)	5.255
Incidence angles	25° to 65°
Spatial resolution	50km
Nodal grid	25km
Orbit cycle	29days
Accuracy of SSM products	0.04-0.08 m ³ m ⁻³
Data availability over Gourma	daily

630
631
632

633
 634
 635
 636
 637
 638

Table 4:
Correlation coefficient (r) and Root Mean Square Error (RMSE) between in-situ measurement of surface soil moisture and S-band backscattering coefficients for the study sites.

Site		Agoufou			Bangui Mallam			Ekia			Kyrnia		
Period		2005-2007			2005-2007			2005-2007			2007		
Mean distance(km)		3			9.5			5.5			3		
SSM depth (cm)		5	10	40	5	10	30	5	10	30	5	10	30
Ice-1	N	25	25	25	20	20	20	22	22	22	8	8	8
	r	0.50 *	0.41 *	0.43 *	0.64 **	0.73 **	0.40	0.70 **	0.82 **	0.80 **	0.68	0.94 **	0.98 **
	RMSE (%)	3.87	6.34	4.97	4.52	3.28	6.77	2.62	1.93	2.14	4.44	1.98	1.34
Ice-2	N	24	24	24	20	20	20	22	22	22	8	8	8
	r	0.68 **	0.66 **	0.70 **	0.75 **	0.62 **	0.58 **	0.73 **	0.83 **	0.80 **	0.76 *	0.97 **	0.99 **
	RMSE (%)	2.4	3.27	2.41	3.37	4.35	4.11	2.41	1.87	2.13	3.54	1.29	0.78
Ocean	N	26	26	26	21	21	21	23	23	23	8	8	8
	r	0.27	0.36	0.41 *	0.65 *	0.64 **	0.34	0.55 **	0.70 **	0.70 **	0.73 *	0.96 **	0.99 **
	RMSE (%)	7.94	7.37	5.19	4.36	4.12	7.88	3.93	2.77	2.86	3.96	1.55	0.84

639 *: significance >95% **: significance >99%

640

Table 5:
Correlation coefficient (r) and Root Mean Square Error (RMSE) between in-situ measurement of surface soil moisture and Ku-band backscattering coefficients for the study sites.

Site		Agoufou			Bangui Mallam			Eguerit	Ekia			Kobou			Kyrnia		
Period		2005-2010			2005-2010			2008-2009	2005-2010			2008-2010			2007-2010		
Mean distance (km)		3			9.5			2	5.5			9.7			3		
SSM depth (cm)		5	10	40	5	10	30	5	5	10	30	5	10	30	5	10	30
Number of samples		56	56	56	27	49	49	13	51	51	51	28	28	28	29	29	29
Ice-1	r	0.85 **	0.85 **	0.55 **	0.7 **	0.73 **	0.3 *	0.95 **	0.59 **	0.63 **	0.55 **	0.52 **	0.33	0.54 **	0.66 **	0.66 **	0.6 **
	RMSE (%)	1.74	1.85	3.29	3.61	3.22	8.35	1.98	3.32	2.84	3.65	5.84	10.8	4.61	4.59	5.09	6.26
Ice-2	r	0.83 **	0.86 **	0.54 **	0.7 **	0.73 **	0.26	0.94 **	0.59 **	0.61 **	0.52 **	0.55 **	0.36	0.54 **	0.66 **	0.64 **	0.52 **
	RMSE (%)	1.85	1.76	3.4	3.54	3.23	9.67	2.36	3.33	2.99	3.94	5.34	10.03	4.66	4.51	5.38	7.79
Sea Ice	r	0.82 **	0.83 **	0.54 **	0.69 **	0.73 **	0.3 *	0.95 **	0.58 **	0.63 **	0.55 **	0.52 **	0.33	0.55 **	0.64 **	0.64 **	0.59 **
	RMSE (%)	1.9	2.02	3.4	3.66	3.19	8.32	2	3.44	2.86	3.61	5.8	10.83	4.55	4.78	5.35	6.53
Ocean	r	0.52 **	0.54 **	0.34 **	0.62 **	0.71 **	0.23	0.95 **	0.46 **	0.54 **	0.56 **	0.55 **	0.39 *	0.58 **	0.53 **	0.49 **	0.45 *
	RMSE (%)	4.52	4.63	5.89	4.38	3.41	11.12	2.05	4.74	3.65	3.6	5.35	8.85	4.25	6.44	8	9.29

*: significance >95% **: significance >99%

1 **Table 6:**
2 **Correlation coefficient (r) and Root Mean Square Error (RMSE) between in-situ measurement of**
3 **surface soil moisture and Ku-band altimetry-derived surface soil moisture estimation for the 3 sandy**
4 **sites of Agoufou, Bangui Mallam and Ekia.**
5
6

Site		Agoufou		Bangui Mallam		Ekia	
In-situ SSM measurement depth (cm)		5	10	5	10	5	10
Ice-1	r	0.88**	0.87**	0.72**	0.73**	0.73**	0.64**
	RMSE (%)	1.39	1.50	3.29	3.79	2.26	2.33
Ice-2	r	0.86**	0.88**	0.76**	0.73**	0.74**	0.64**
	RMSE (%)	1.62	1.53	2.35	2.93	2.40	2.70
Sea Ice	r	0.87**	0.85**	0.71**	0.74**	0.72**	0.66**
	RMSE (%)	1.44	1.58	3.03	3.36	2.22	2.21
Ocean	r	0.69**	0.68**	0.65**	0.71**	0.49**	0.54**
	RMSE (%)	3.15	3.26	2.76	2.52	3.16	2.99

7 *: significance >95% **: significance >99%

10
11
12
13
14
15
16

Table 7:

Correlation coefficients (r), bias and RMSE between ASCAT SSM products and RA-2 Ku-band derived SSM for 3 study sites (Agoufou, Bangui-Mallam and Ekia).

Site		Agoufou		Bangui Mallam		Ekia	
Inversion function (depth in cm)		5	10	5	10	5	10
Ice-1	r	0.49*	0.47*	0.30	0.30	0.42	0.43
	RMSE (%)	4.92	4.92	4.04	3.95	10.41	9.25
	bias	0.9062	0.72	-0.90	-1.18	-8.01	-6.77
Ice-2	r	0.56*	0.54*	0.39	0.39	0.48*	0.48*
	RMSE (%)	4.59	4.67	3.70	3.65	7.98	7.45
	bias	1.48	1.09	-0.99	-1.46	-6.97	-6.56
Sea Ice	r	0.49*	0.47*	0.30	0.30	0.43	0.43
	RMSE (%)	4.89	4.91	3.99	3.91	9.83	8.79
	bias	0.91	0.69	-0.99	-1.29	-7.35	-6.31
Ocean	r	0.50*	0.50*	0.29	0.29	0.45	0.45
	RMSE (%)	4.82	4.83	3.72	3.71	5.45	5.43
	bias	0.3135	-0.0865	-1.21	-1.64	-4.51	-4.78

*: significance >95% **: significance >99%

17
18

Figure captions

Fig. 1: The AMMA-CATCH mesoscale site in Mali, showing the 6 automatic soil moisture stations (squares) and ENVISAT path 302 (black line).

Fig. 2: Spatial variations of the backscattering coefficient along the ENVISAT RA-2 groundtrack 302 for dry (January - April) and wet (JJAS) seasons using Ice-1 algorithm. a) Ku band; b) S band. Image from Google-Earth is shown for comparison.

Fig. 3: Space-time diagram of ENVISAT RA-2 data over the AMMA-CATCH mesoscale window with Ku-band Ice-1 backscattering coefficient values for a sampling rate in latitude of 0.008° (about 1 km). Blank stripes correspond to missing or corrupted values. a) Ku-band (2002-2010); b) S- band (2002-2007).

Fig. 4: Time variation of volumetric soil moisture in % (—), and Ice-1 algorithm backscattering coefficient σ_0 in dB for S-band (---) and Ku-band (---) at Agoufou site for year 2007. a) Soil moisture measurements at 5cm depth; b) Soil moisture measurements at 10cm depth and c) soil moisture measurements at 40cm depth.

Fig. 5: Temporal variations of Ku-band Ice-1 backscattering coefficient σ_0 (—) in dB and volumetric soil moisture (SSM in %) at 5cm depth (- - -) over the period January 2005 - October 2010. a) Ekia ; b) Eguerit; c) Bangui Mallam; d) Agoufou; e) Kyrnia; f) Kobou.

Fig. 6: Scatterplot of Ku-band Ice-1 backscattering coefficient σ_0 (in dB) versus volumetric soil moisture (SSM in %) at 5cm depth. Correlation coefficient (r), Root Mean Square Error (RMSE) in % of soil moisture, and number of data (n) are also indicated. a) Ekia; b) Eguerit; c) Bangui Mallam; d) Agoufou; e) Kyrnia; f) Kobou.

Fig. 7: Scatterplot of backscattering coefficient σ_0 (Ice-1 algorithm) versus Leaf Area Index (LAI) for the Agoufou site. Correlation coefficients (r) and number of samples (n) for $LAI > 0.2$ are given for the period 2005-2010. The linear equation is indicated.

Fig. 8: Linear regression of the Ice-1 normalized backscattering coefficient σ_0 versus volumetric soil moisture at 5 cm for the sandy sites. The mean sandy site regression equation is indicated, along with the number of samples considered (n), the correlation coefficient (r) and the Root Mean Square Error (RMSE) given in % of soil moisture.

45 Fig. 9: Time variation of the volumetric soil moisture at Agoufou, measured at 5cm depth (plain line) and
46 estimated (circles with error bars) using the general σ_0 - SSM relationships for sandy soils for Ice-1
47 backscattering coefficients. Are also indicated the number of samples considered (n), the correlation
48 coefficient (R) and the Root Mean Square Error (RMSE) given in % of soil moisture.

49 Fig. 10: Time variation of ASCAT SSM product and ENVISAT Ice-1 SSM estimation for the Agoufou site
50 from 2007 to 2010, with the corresponding error bars. Are also indicated the number of samples considered
51 (n), the correlation coefficient (r) and the Root Mean Square Error (RMSE) given in % of soil moisture.

52

Fig. 1

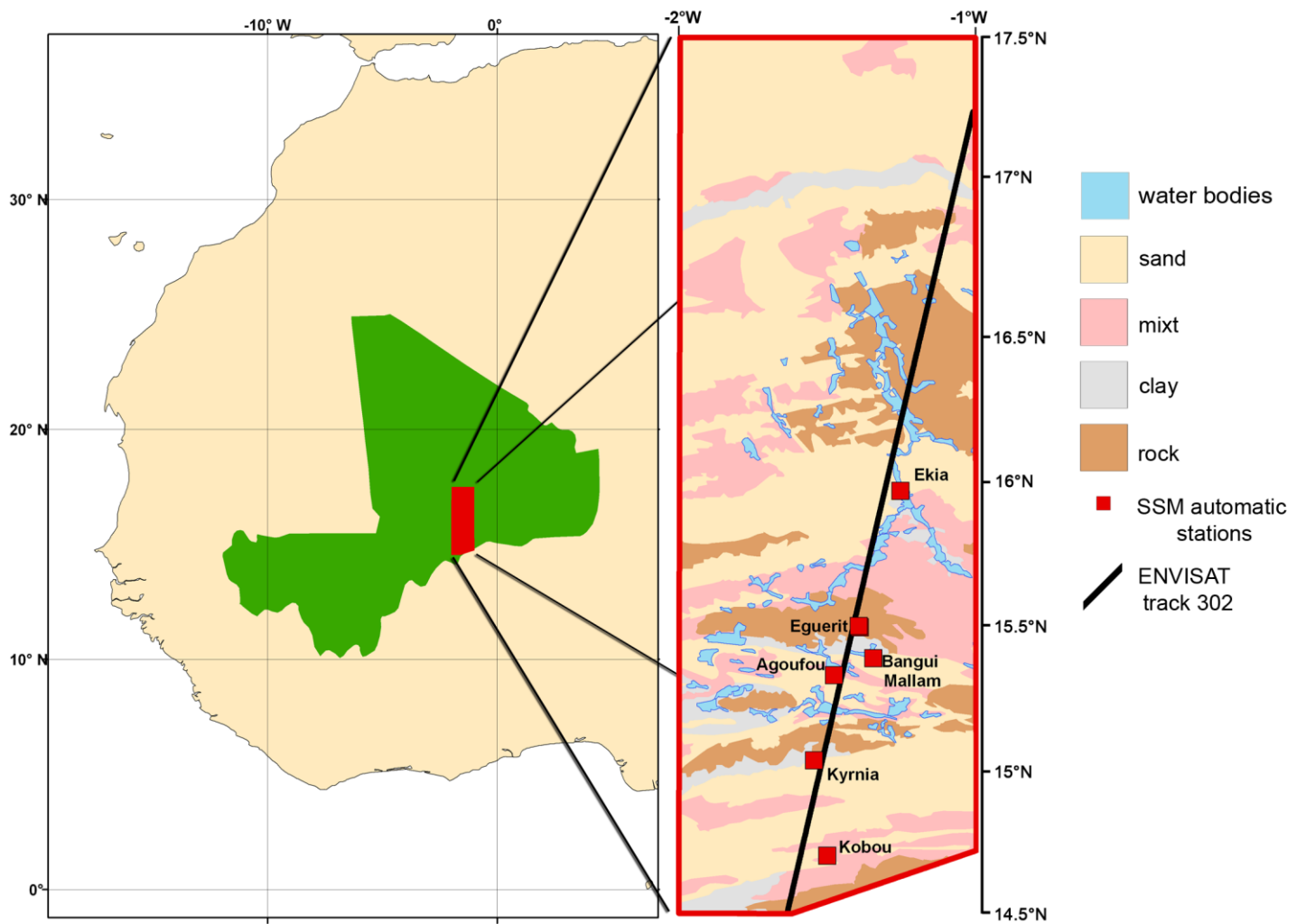
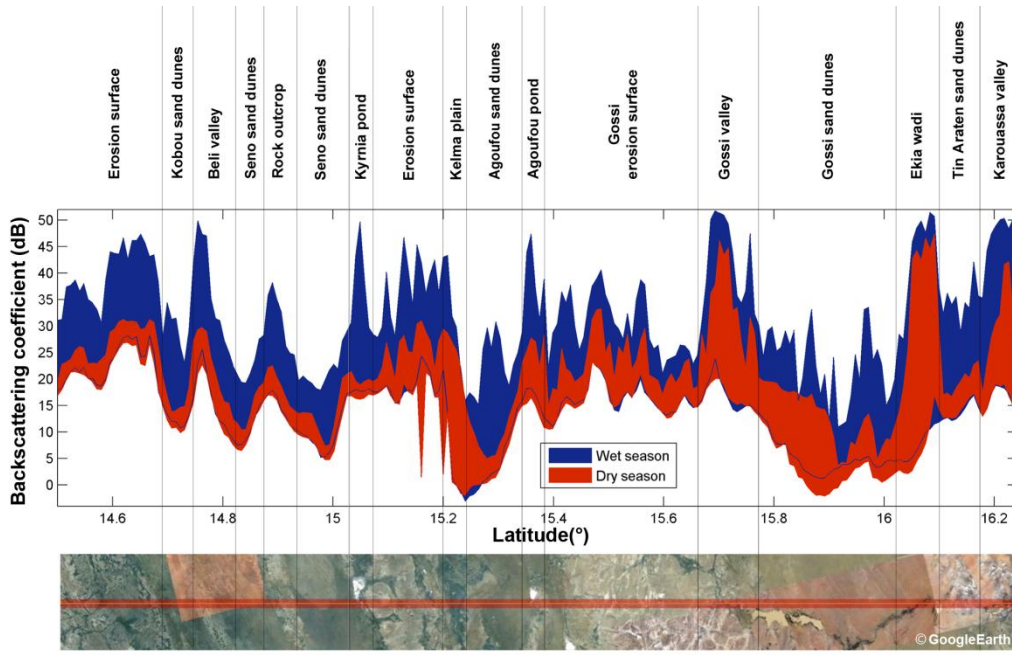
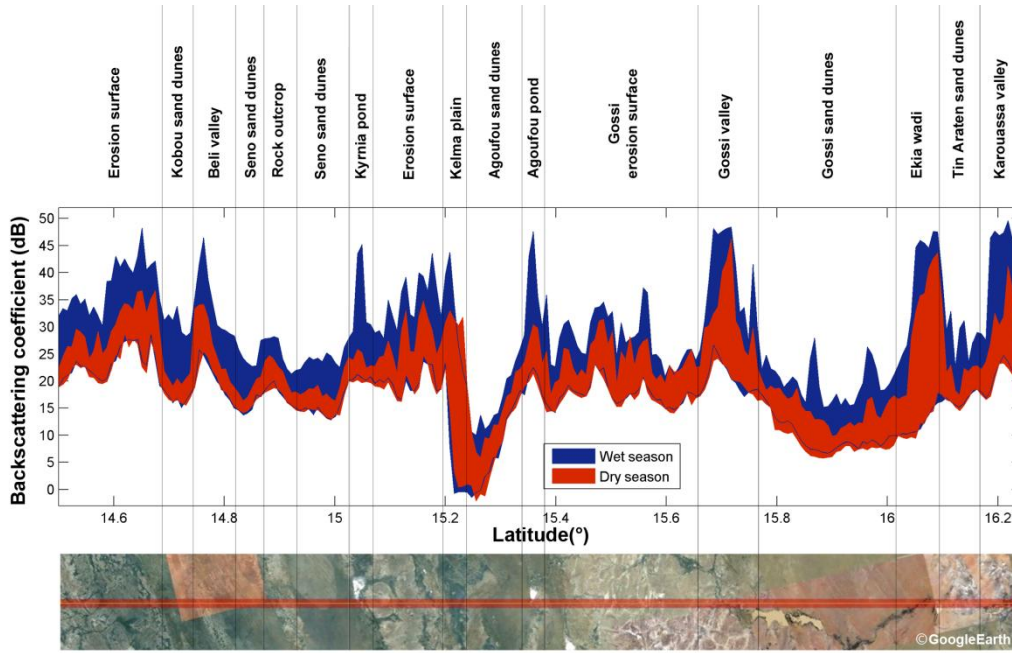


Fig. 2



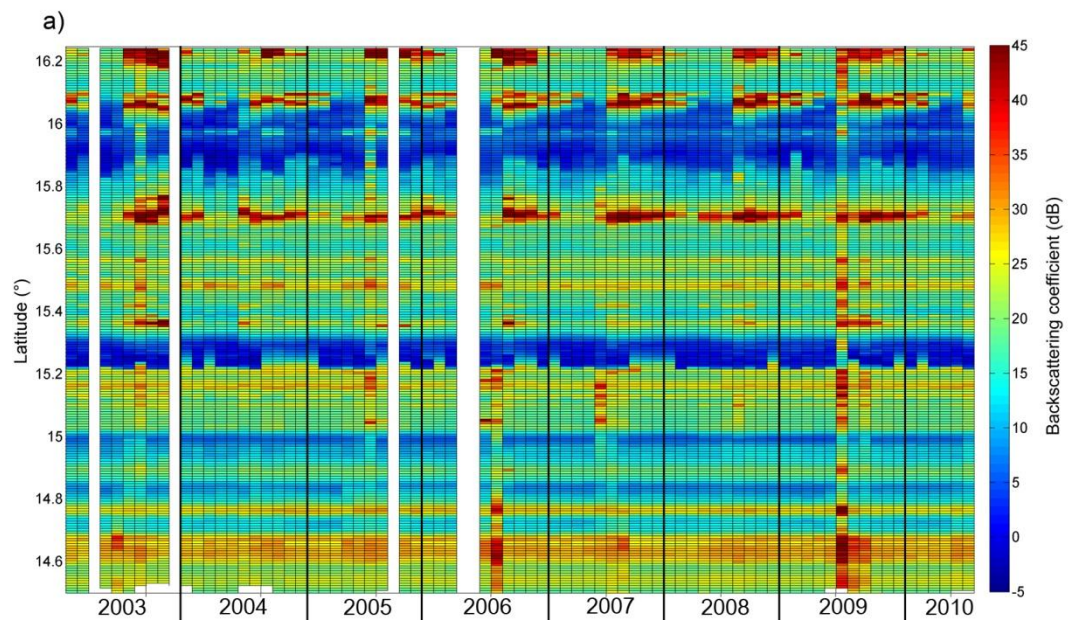
a) Ku band



b) S band

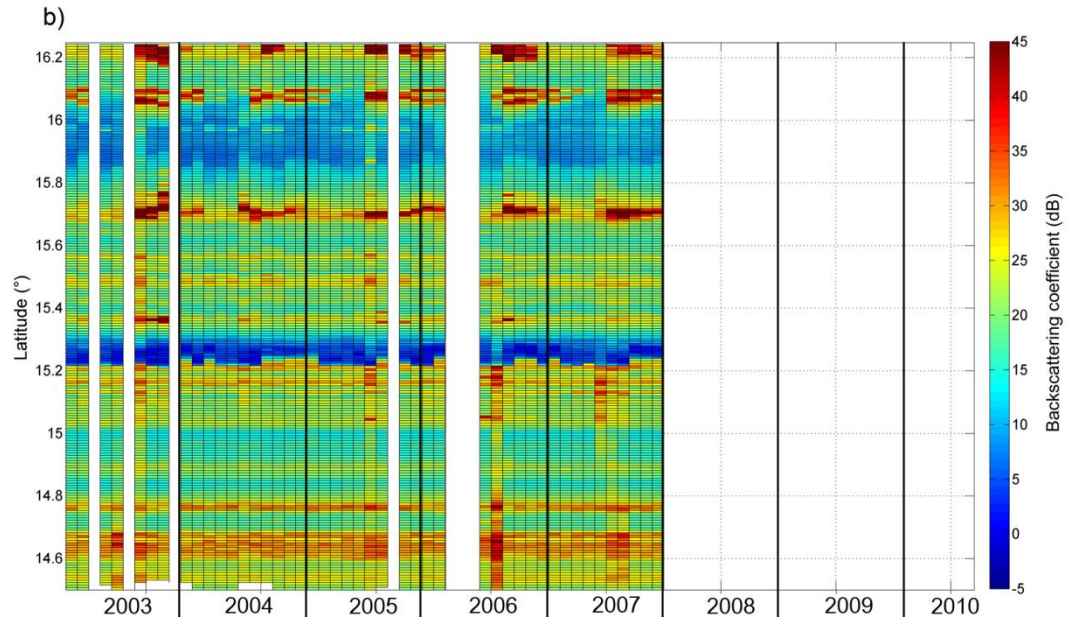
70

Fig. 3



71

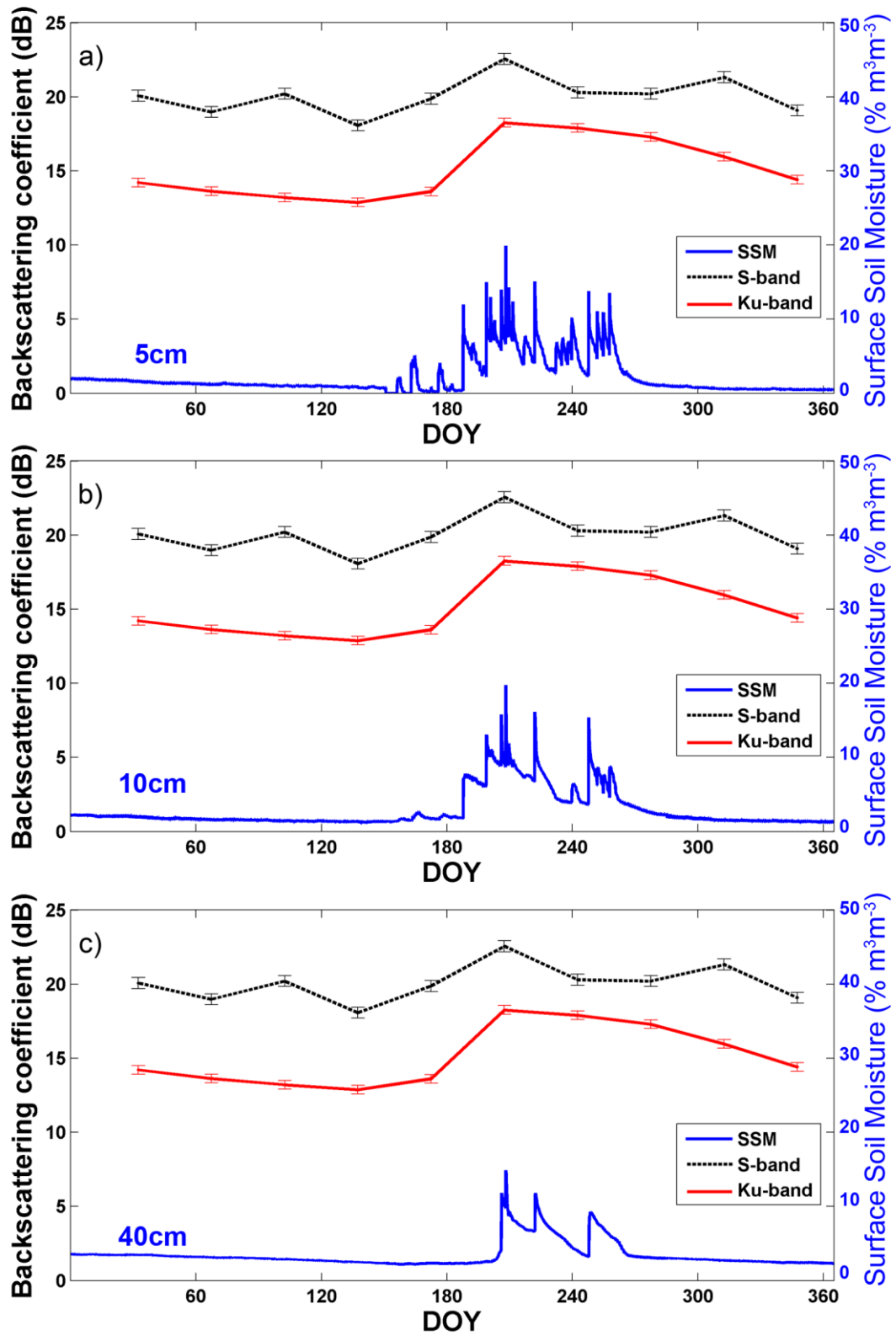
72



73

74

Fig. 4

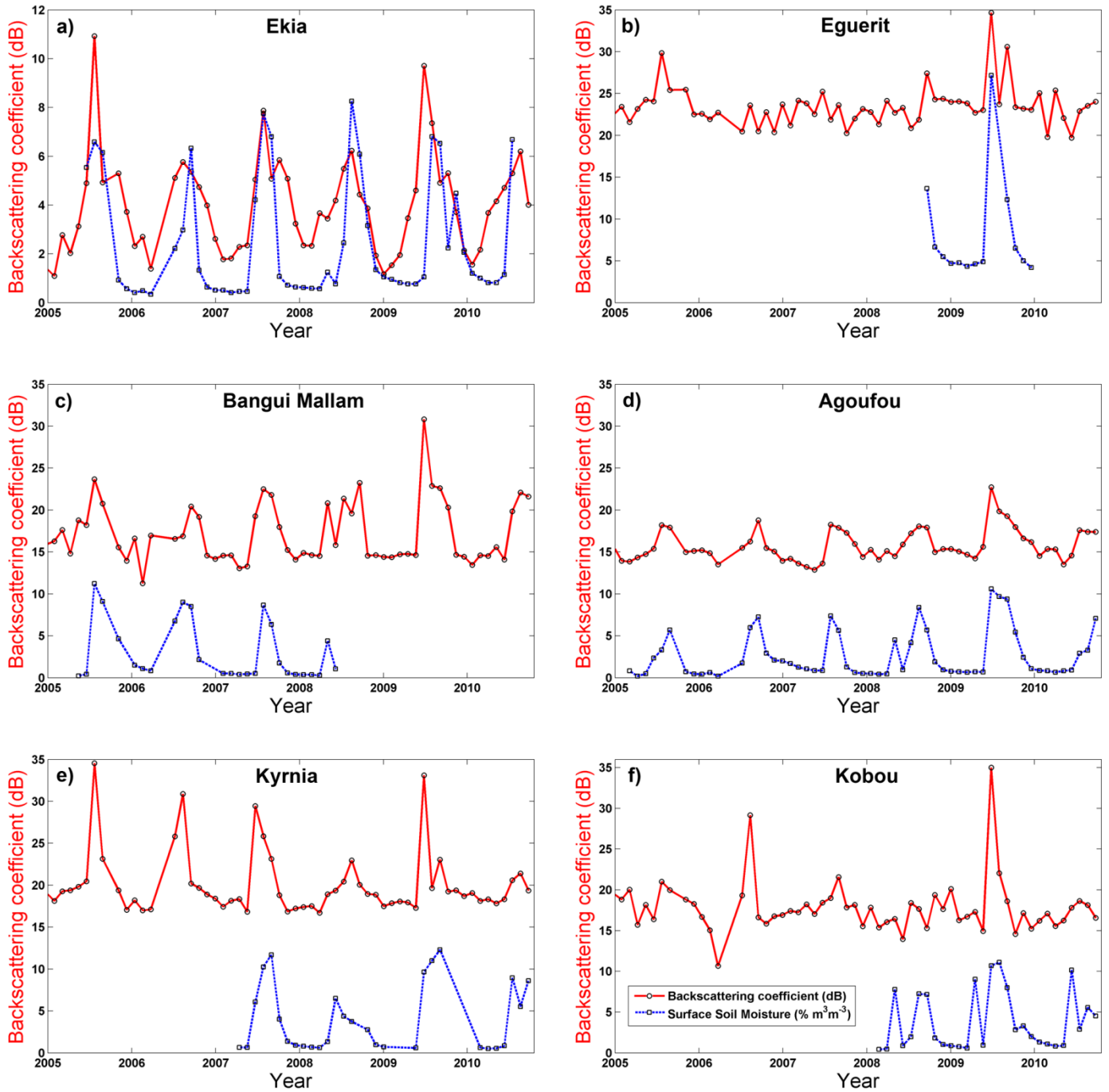


75
76

77
78
79
80

81
82
83

Fig. 5



84
85
86
87

Fig. 6

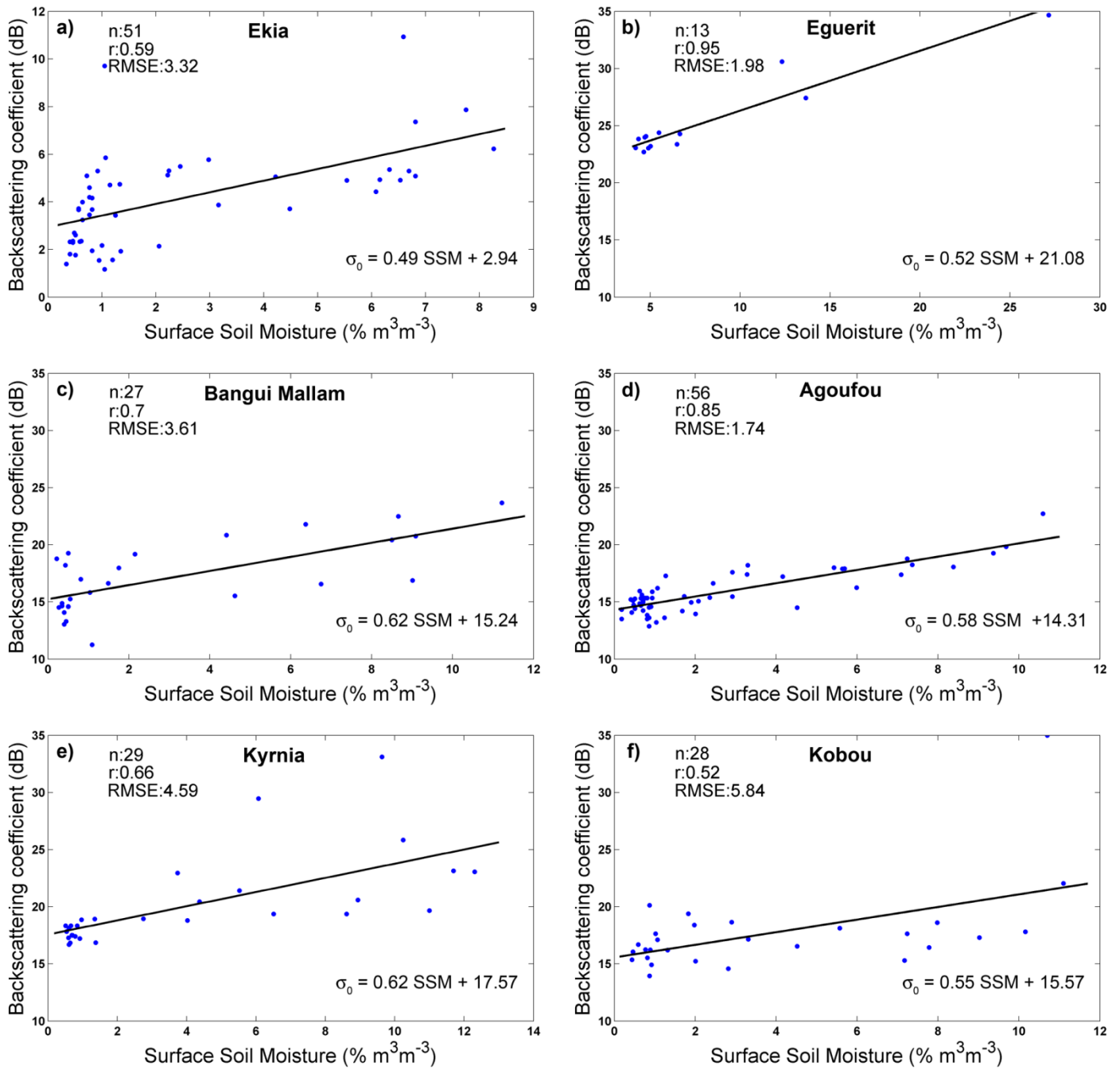
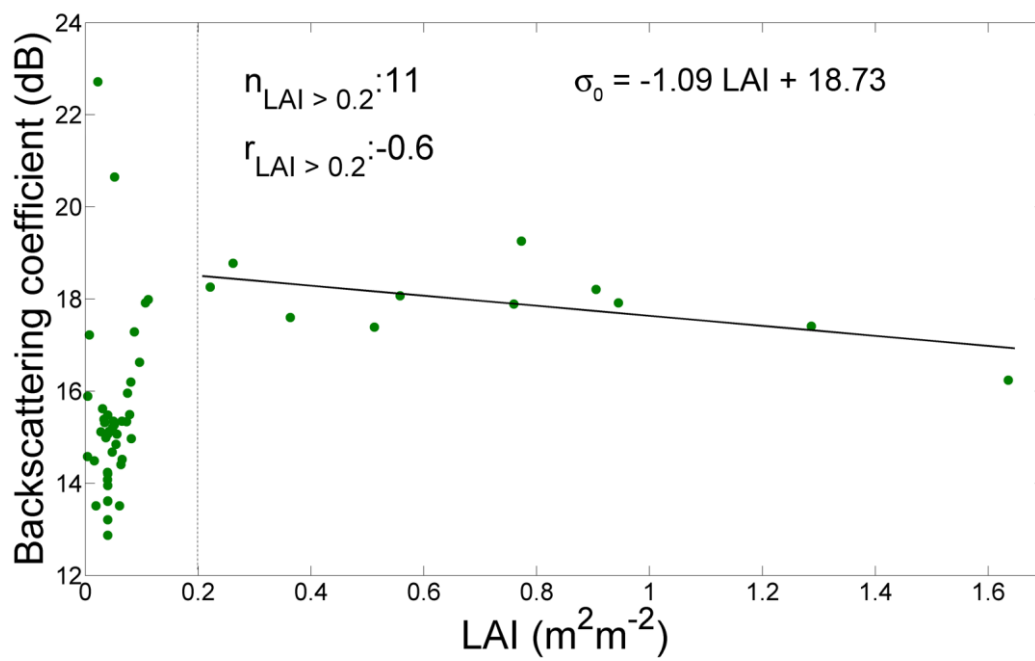


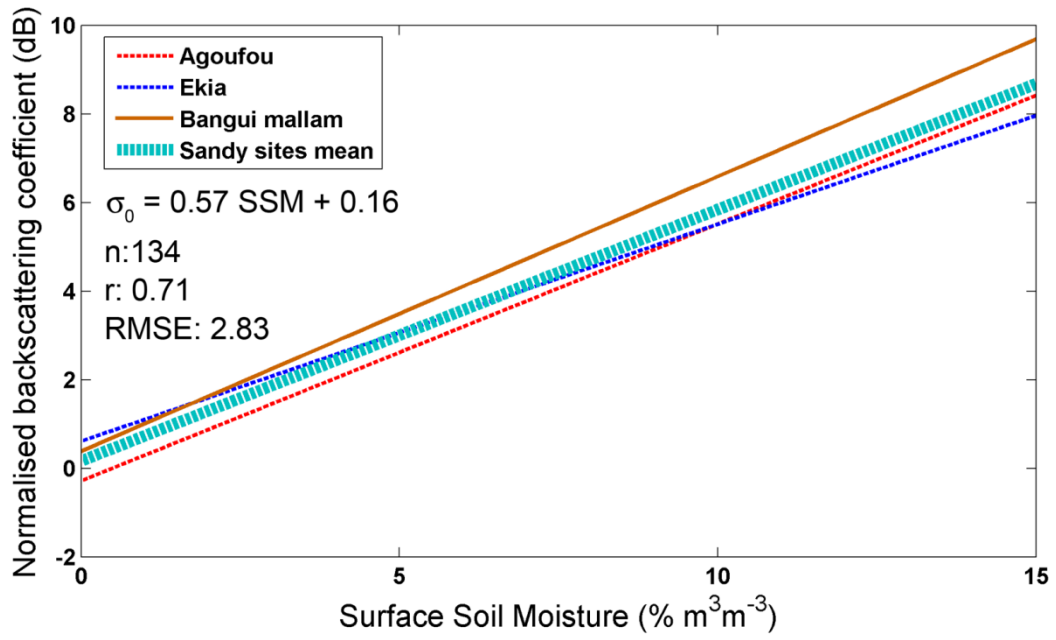
Fig. 7



98
99
100
101

102
103
104
105
106

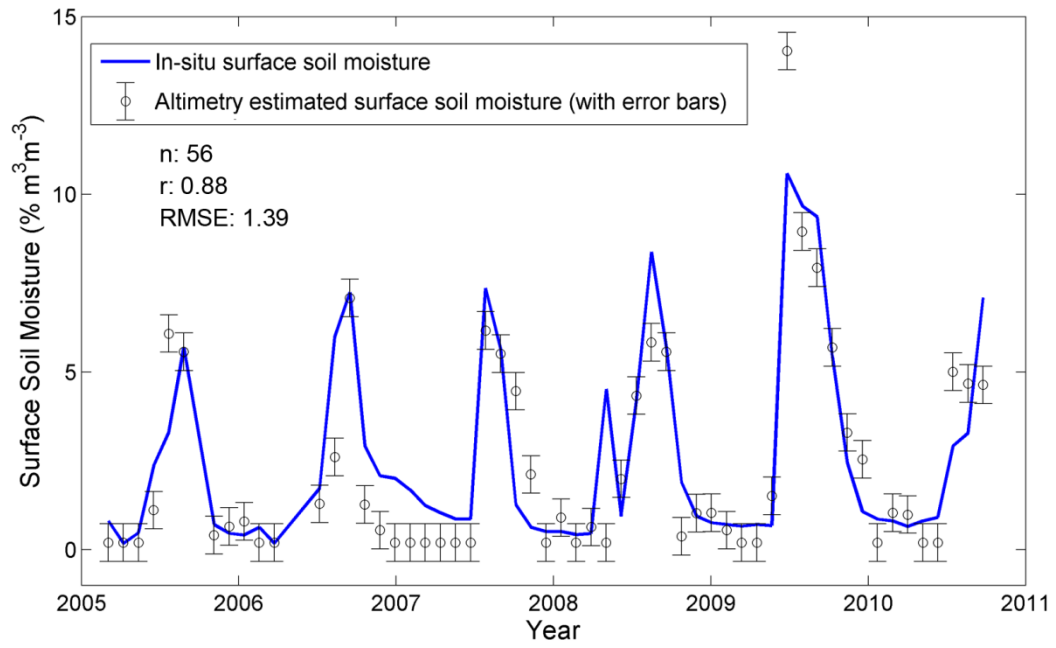
Fig. 8



107
108

109
110
111

Fig. 9

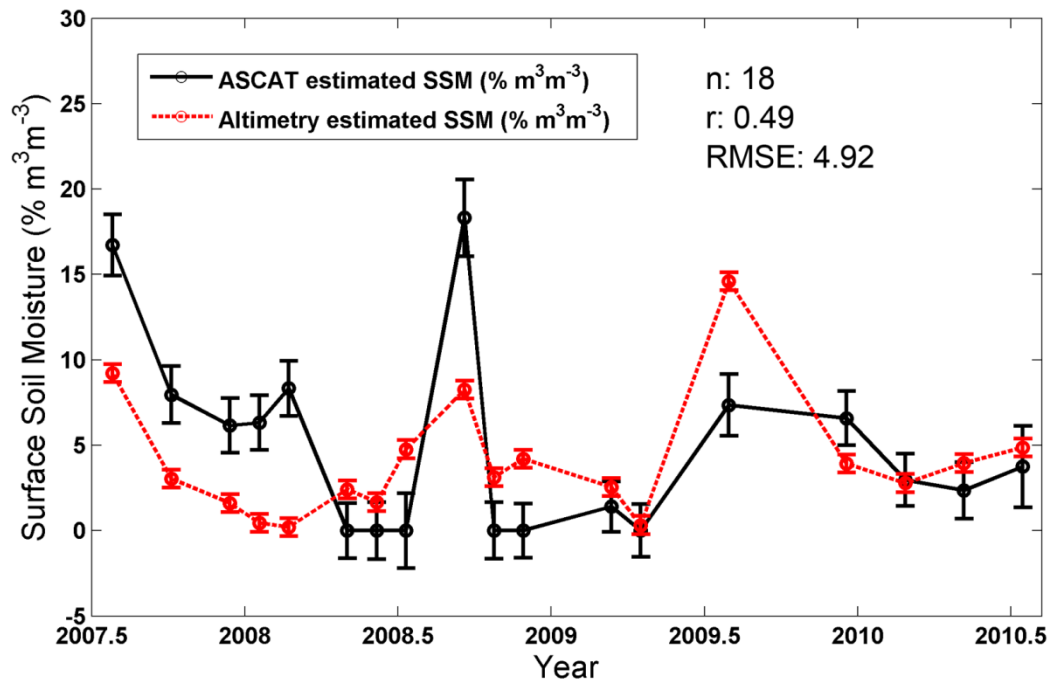


112
113

114

Fig. 10

115



116